HHS Public Access

Author manuscript

*Dev Dyn*. Author manuscript; available in PMC 2024 March 18.

Published in final edited form as:

*Dev Dyn*. 2023 April ; 252(4): 510–526. doi:10.1002/dvdy.560.

# Identification of HSPA8 as an interacting partner of MAB21L2 and an important factor in eye development

**Sarah E. Seese**[1,2], **Sanaa Muheisen**[1], **Natalie Gath**[3], **Jeffrey M. Gross**[3], **Elena V. Semina**[1,2,4,5,#]

[1]Department of Pediatrics The Medical College of Wisconsin, Milwaukee, WI 53226, USA

[2]Cell Biology, Neurobiology and Anatomy, The Medical College of Wisconsin, Milwaukee, WI 53226, USA

[3]University of Pittsburgh School of Medicine, Pittsburgh, PA 15213, USA

[4]Department of Ophthalmology and Visual Sciences, Medical College of Wisconsin, Children's of Wisconsin, Milwaukee, WI 53226, USA

[5]Children's Research Institute, Medical College of Wisconsin, Children's of Wisconsin, Milwaukee, WI 53226, USA

## Abstract

**Background:** Pathogenic variants in human *MAB21L2* result in microphthalmia, anophthalmia and coloboma. The exact molecular function of MAB21L2 is currently unknown. We conducted a series of yeast two-hybrid (Y2H) experiments to determine protein interactomes of normal human and zebrafish MAB21L2/mab21l2 as well as human disease-associated variant MAB21L2-p.(Arg51Gly) using human adult retina and zebrafish embryo libraries.

**Results:** These screens identified klhl31, tnpo1, TNPO2/tnpo2, KLC2/klc2, and SPTBN1/sptbn1 as co-factors of MAB21L2/mab21l2. Several factors, including hspa8 and hspa5, were found to interact with MAB21L2-p.Arg51Gly but not wild-type MAB21L2/mab21l2 in Y2H screens. Further analyses via 1-by-1 Y2H assays, co-immunoprecipitation and mass spectrometry revealed that both normal and variant MAB21L2 interact with HSPA5 and HSPA8. *In situ* hybridization detected co-expression of *hspa5* and *hspa8* with *mab21l2* during eye development in zebrafish. Examination of zebrafish mutant $hspa8^{hi138Tg}$ identified reduced *hspa8* expression associated with severe ocular developmental defects, including small eye, coloboma, and anterior segment dysgenesis. To investigate the effects of *hspa8* deficiency on the $mab21l2^{Arg51\_Phe52del}$ allele, corresponding zebrafish double mutants were generated and found to be more severely affected than single mutant lines.

**Conclusion:** This study identifies heat shock proteins as interacting partners of MAB21L2/mab21l2 and suggest a role for this interaction in vertebrate eye development.

### Keywords

HSPA8; HSPA5; MAB21L2; co-factor; coloboma; zebrafish

[#]To whom correspondence should be addressed: esemina@mcw.edu.

## Introduction

Pathogenic variants in *MAB21L1* and *MAB21L2* of the male-abnormal 21 like family have been shown to cause human ocular developmental disorders. Dominant and recessive alleles in *MAB21L2* were identified in several families with microphthalmia, anophthalmia or coloboma (MAC) [1–5]. For dominant alleles, various missense variants affecting the same arginine residue at position 51 were most common (4/7 dominant families) [2,3,5]. For *MAB21L1*, recessive alleles (both missense and presumed loss-of-function) were associated with cerebello-oculo-facio-genital syndrome in six unrelated families, where the main ocular features include corneal dystrophy/opacities and nystagmus [6,7]. More recently, our group reported additional *MAB21L1* alleles in patients with microphthalmia, coloboma and aniridia, including a dominant allele affecting the same arginine residue at position 51, p.(Arg51Leu), conserved in all MAB21L proteins [8].

The functional roles of MAB21L proteins are still largely unknown. The solved crystal structure for MAB21L1 suggested possible nucleotidyltransferase (NTase) activity due to a high amount of structural overlap with a known NTase, cyclic GMP-AMP synthase (cGAS), involved in cytosolic DNA recognition and subsequent synthesis of second messenger cGAMP [9–11]. However, *in vitro* experiments have been unable to provide evidence supporting this activity [5,10]. A role in transcriptional regulation has also been proposed as both Mab21l1 and Mab21l2 have been shown to localize to the nucleus [12] and to have mild affinity for nucleic acids, in particular single-stranded RNA [5,10]. In addition, MAB21L2 showed transcriptional repressor/co-repressor activity in one study based on *in vitro* luciferase assays [13]. Further data has supported a role for Mab21l1/Mab21l2 in Tgf-β signaling [13,14] and/or the Pax6 pathway [15–18].

One way to gain insight into a protein's function(s) is to discern its possible interactions using a large-scale unbiased approach. To identify critical interactions of MAB21L2 involved in disease pathogenesis, we used a yeast two-hybrid screen to compare the interactome of human and zebrafish wild-type MAB21L2/mab21l2 and p.(Arg51Gly) mutant and identified several heat shock proteins (HSP) including HSPA8/hspa8 and HSPA5/hspa5 as major interactants. Furthermore, we utilized the zebrafish model to reveal the importance of *hspa8* in ocular development by itself and in a *mab21l2*-deficient background.

## Results

### Identification of candidate co-factors of MAB21L2 by Y2H screening

Yeast two-hybrid analyses were conducted as an unbiased approach to identify potential binding partners of the human/zebrafish MAB21L2/mab21l2 wild-type and human p.(Arg51Gly) mutant proteins (Table S1). MAB21L2 proteins are highly conserved with matching lengths (359 aa) and 97% (348/359) identify at the protein level between human and zebrafish. Two libraries were selected for this experiment, 1) human retina (adult), to identify interactions relevant to human retina and 2) zebrafish embryo (18-20 hpf), to capture important interactions taking place during vertebrate embryonic development.

In the screens, MAB21L2-WT versus human retina library tested 77.5 million interactions and isolated 156 positive clones; MAB21L2-WT versus zebrafish embryo (18-20 hpf) library tested 61.6 million interactions and isolated 356 positive clones; MAB21L2-p.(Arg51Gly) versus zebrafish embryo (18-20-hpf) library tested 36.3 million interactions and isolated 268 positive clones; and mab21l2-wt versus zebrafish embryo (18-20 hpf) library tested 58.6 million and 74 million interactions and identified 86 and 234 positive clones (using a LexA and GAL4 DNA binding domain, respectively) (Table S1). To note, two screens, MAB21L2-p.(Arg51Gly) versus zebrafish embryo library and mab21l2-wt (pB27 vector) versus zebrafish embryo, resulted in mild autoactivation of the *HIS3* reporter gene and thus were treated with 3-AT, resulting in a reduced number of tested interactions due to higher selective pressure.

The results were first prioritized based on confidence score, with a focus on those with A-D scores (Table S2). Then, interactions which appeared in two or more independent wild-type screens were selected for further analysis, which included 30 factors (Table 1). In this list, we noted several interactions that appeared in three or more independent screens and had a confidence score of A or B in at least one of these screens, and that had overlapping selected interaction domains (SID; region that was shared for all prey mapping to the same reference protein) between screens, increasing the possibility that these were relevant findings. This included kelch-like protein 31 (klhl31), transportin-1 (tnpo1) and transportin-2 (TNPO2/tnpo2), kinesin light chain 2 (KLC2/klc2) and spectrin beta chain (SPTBN1/sptbn1) (Table 1). Previous data demonstrated that both wild-type MAB21L2 [2,12] and MAB21L2-p.(Arg51Gly) [2] variant display primarily nuclear localization. Analysis of available subcellular localization data revealed that half of all prioritized factors (15/30) and four out of the five most consistent interactants between screens, klhl31, tnpo1, tnpo2, and SPTBN1/sptbn1, were reported to have nuclear staining (uniprot.org; [19]) and thus are likely to co-localize with MAB21L2 in the cell. The remaining protein, KLC2/klc2, has not been observed in the nucleus; however, since MAB21L2 also demonstrates some cytoplasmic staining [12], this interaction cannot be excluded. All five of these most consistent interacting partners exhibited high confidence scores with both wild-type MAB21L2/mab21l2 and mutant MAB21L2-p.(Arg51Gly), indicating that these interactions are not disrupted by the pathogenic variant.

Dominant mutations in *MAB21L2* have been hypothesized to have gain-of-function effects [5]. Therefore, to identify interactions unique to the mutant, factors interacting with MAB21L2-p.(Arg51Gly) with high confidence (A-D) scores but not showing a similar binding to the wild-type protein in all three independent screens were selected (Table 2). A total of 27 interactions were detected exclusively for the mutant; of these, only one A-level interaction was identified (hspa8), one B-level (gfm1) and four C-level (hspa5, sfpq, kif4 and blzf1). Notably, two heat shock proteins were present in this short list, heat shock cognate 71 kDa protein (hspa8) and heat-shock 70 kDa protein 5 (hspa5), both with noted nuclear staining (uniprot.org; [20–23]) and thus consistent with MAB21L2/MAB21L2-p.(Arg51Gly) primary subcellular localization [2,12]. The interacting fragment of hspa8 involved amino acids 255-420 (which contains two (out of four) ATP-binding subdomains and a part of the substrate-binding domain (uniprot.org; [24])), while for MAB21L2-p.(Arg51Gly) it is

unclear what specific region was involved in the interaction since the entire protein was used as a bait.

To verify the Y2H data, 1-by-1 interaction assays were conducted in yeast including the zebrafish hspa8 fragment isolated from the initial Y2H screen (nucleotides 762-1494) that was tested against human MAB21L2-WT and MAB21L2-p.(Arg51Gly). Interestingly, the interaction was confirmed for both MAB21L2-p.(Arg51Gly) (Figure 1B), along with MAB21L2-WT (Figure 1A). This is contrary to the results of the Y2H, where the interaction was only identified for the mutant protein. However, yeast growth was stronger for the mutant; this growth difference could be indicative of differing affinities between mutant and wild-type MAB21L2 with hspa8.

## Validation of Y2H data in mammalian cells

To explore MAB21L2 interactions in mammalian cells, we performed mass spectrometry analysis of proteins co-immunoprecipitated with either wild-type or mutant (p.(Arg51Gly)) FLAG-tagged MAB21L2 proteins in HLE-B3 human lens epithelial cells. 91 and 107 proteins were found to be significantly enriched in precipitates obtained with wild-type and mutant MAB21L2 proteins, correspondingly (Tables S4 and S5). When the mass spectrometry and Y2H data were compared, a total of 6 proteins were found to overlap, DSP, SPTBN1, VPS35, HSPA5, HSPA8 and HSP90B1 (Table S3). For HSPA8, an abundance ratio of 74.817 was identified when comparing MAB21L2-p.(Arg51Gly) transfected to untransfected cells and 58.74 when comparing MAB21L2 wild-type transfected to untransfected cells (1.274 mutant/WT abundance ratio), suggesting a stronger interaction between HSPA8 and the MAB21L2 mutant but not significantly different (P value 0.099) (Table S3). For HSPA5, abundance ratios of 13.927 for MAB21L2-p.(Arg51Gly) mutant and 17.106 for wild-type MAB21L2 transfected cells/untransfected controls were identified (0.814 abundance ratio; P value 0.813).

To further validate human full-length HSPA8 and HSPA5 interactions against MAB21L2-WT and p.(Arg51Gly), co-immunoprecipitation (co-IP) was performed. The myc-tagged HSPA8 (n=6 experiments; Figure 1C) and myc-tagged HSPA5 (n=2 experiments; Figure 1D) were both immunoprecipitated with FLAG-tagged MAB21L2-WT as well as MAB21L2-p.(Arg51Gly).

## hspa8 and hspa5 expression in zebrafish

To investigate the expression of *hspa8* and *hspa5* during zebrafish ocular development *in situ* hybridization was performed on 24, 48 and 96-hpf embryos. Both *hspa5* and *hspa8* demonstrated broad expression patterns at all embryonic stages, including strong presence during eye development. The expression of *hspa8* and *hspa5* was enriched in the developing eye, retinal ciliary marginal zone, and lens, as well as the brain and craniofacial regions, overlapping *mab21l2* expression domains (Figure 2). The co-expression of *mab21l2* and *hspa* genes during embryonic development supports the possibility of functionally important interaction between the encoded proteins.

### hspa8$^{hi138Tg/hi138Tg}$ embryos demonstrate reduced level of hspa8 transcript

To explore the role of *hspa8* in zebrafish ocular development, we obtained a mutant line from the Zebrafish International Resource Center (ZIRC), *hspa8*$^{hi138Tg}$. This line was generated via a large-scale retroviral-mediated insertional mutagenesis screen [25] using established protocols [26]. Genomic DNA sequencing confirmed the location of the retroviral insert 350 bps upstream of the *hspa8* 5' untranslated region (UTR).

To identify the effect of the 5' insertion on *hspa8* expression, RT-PCR was performed on 48-hpf embryos. In comparison to wild-type embryos, homozygous *hspa8*$^{hi138Tg}$ embryos exhibited a noticeable reduction in *hspa8* expression (Figure 3A). To further validate these results, qRT-PCR was performed. Significant reduction in *hspa8* expression was observed with both primer pairs tested with the following results: exon 2 – exon 3: −404.6 fold-change, $P<0.0001$; exon 2 – exon 4: −281.1 fold-change, $P<0.0001$ (Figure 3B).

### hspa8$^{hi138Tg/hi138Tg}$ embryos show ocular abnormalities

Homozygous embryos were identified in ~25% of progeny from heterozygous adult crosses, consistent with the principles of Mendelian inheritance. Previous observations of homozygous *hspa8*$^{hi138Tg}$ mutants at 5-dpf had identified gross abnormalities of the hindbrain, thinner body with a rounder yolk, underdevelopment of the liver/gut, small head with central nervous system necrosis, and small eyes [25,27]. We examined homozygous offspring at early developmental stages (24-72-hpf) with an emphasis on ocular structures and noted the following phenotypes: small eyes with variable coloboma and anterior segment anomalies (thickened developing cornea and absent anterior chamber space at 72-hpf) (Figure 3C–I'); ocular features were correlated with embryos with more severe coloboma displaying more significant anterior segment defects. Heterozygous eyes appeared normal at all stages. Progeny from heterozygous crosses were reared to adulthood; genotyping revealed no surviving homozygotes, suggesting lethality, with normal survival and morphology for heterozygous *hspa8*$^{hi138Tg}$ adults.

To further assess the ocular phenotype, we performed histological analysis on 24-, 48- and 72-hpf wild-type (9, 10 and 9 eyes, respectively) and *hspa8*$^{hi138Tg}$ homozygous mutants (4, 5 and 6 eyes, respectively) (Figure 3J–L'). At 24-hpf, smaller eyes with cornea-lenticular adhesions and abnormal retinal morphology were observed. At 48- and 72-hpf, mutant eyes show aberrant retina lacking any signs of retinal lamination, abnormally thick corneas, and absent anterior chamber.

### Genetic interaction of hspa8 and mab21l2 alleles in zebrafish

In order to examine the genetic interaction between *mab21l2* and *hspa8*, double mutants carrying *hspa8*$^{hi138Tg}$ [25] and *mab21l2*$^{mw702}$ (*mab21l2*$^{Arg51\_Phe52del}$) alleles were generated. The *mab21l2*$^{mw702}$ allele is an in-frame deletion of two amino acids including the arginine at position 51, c.151_156delCGTTTC, p.(Arg51_Phe52del); fish homozygous for this allele display coloboma [2]. Double heterozygous adults, *hspa8*$^{hi138Tg/+}$: *mab21l2*$^{mw702/+}$, were crossed to generate different combinations of *hspa8*$^{hi138Tg}$ and *mab21l2*$^{mw702}$ alleles. Phenotyping of the ventral retina/optic fissure region and lens was completed for the following numbers of eyes for each genotype at 48-hpf: *hspa8*$^{+/+}$:*mab21l2*$^{+/+}$ 12

eyes, *hspa8*$^{hi138Tg/+}$:*mab21l2*$^{+/+}$ 10 eyes, *hspa8*$^{+/+}$:*mab21l2*$^{mw702/+}$ 15 eyes, *hspa8*$^{hi138Tg/+}$:*mab21l2*$^{mw702/+}$ 20 eyes, *hspa8*$^{hi138Tg/hi138Tg}$:*mab21l2*$^{+/+}$ 5 eyes, *hspa8*$^{+/+}$:*mab21l2*$^{mw702/mw702}$ 32 eyes, *hspa8*$^{hi138Tg/hi138Tg}$:*mab21l2*$^{mw702/+}$ 10 eyes; *hspa8*$^{hi138Tg/+}$:*mab21l2*$^{mw702/mw702}$ 11 eyes, *hspa8*$^{hi138Tg/hi138Tg}$:*mab21l2*$^{mw702/mw702}$ 4 eyes).

Most single and double heterozygous embryos showed a complete fusion of the optic fissure (Figure 4). For single homozygous embryos, most/all fish demonstrated coloboma phenotypes: *hspa8*$^{+/+}$;*mab21l2*$^{mw702/mw702}$ fish displayed grade 1 (25%), grade 2 (46.9%) and grade 3 (21.9%) colobomas with small number of normal eyes (6.2%), while *hspa8*$^{hi138Tg/hi138Tg}$:*mab21l2*$^{+/+}$ embryos all had coloboma with equal numbers (40%) for grade 1 and 2, and 20% for grade 3 (Figure 4G). Embryos with heterozygosity for one gene and homozygosity for another one showed the following results: *hspa8*$^{hi138Tg/+}$:*mab21l2*$^{mw702/mw702}$ eyes had a similar distribution to *hspa8*$^{+/+}$:*mab21l2*$^{mw702/mw702}$ while *hspa8*$^{hi138Tg/hi138Tg}$;*mab21l2*$^{mw702/+}$ embryos showed a more severe coloboma phenotype in comparison to *hspa8* homozygotes in wild-type background with 10% grade 1, 50% grade 2, 20% grade 3 and 20% grade 4. Embryos double homozygous for *hspa8* and *mab21l2* demonstrated the most severe abnormalities, with moderate to severe coloboma in all (75% ranking as grade 4 and the remaining 25% grade 3) (Figure 4G).

To characterize the lens phenotype, we measured lens area in different genotypic groups and observed significant differences. Single heterozygous or homozygous embryos for *mab21l2* showed no significant difference from wild-type, consistent with previous observations [2], while single heterozygous or homozygous embryos for *hspa8* displayed smaller lenses (at 87.9% and 62.5% of wt, respectively) (Figure 4H). Interestingly, embryos with homozygosity for *mab21l2* in *hspa8* heterozygous background showed smaller lenses with a significant difference from wild-type, *mab21l2* homozygotes in wild-type background and *hspa8* heterozygotes, suggesting that interaction between the mutant alleles in these fish produced the abnormal lens size. Consistent with this, double homozygous embryos were the most affected and showed significant differences from all other groups.

## Discussion

Previous work has shown that pathogenic variants in the *MAB21L2* gene are associated with MAC-spectrum ocular phenotypes [1–5]. However, to date, the function(s) of the MAB21L2 protein remain elusive, and knowledge of binding partners is limited. In this study we have identified potential cofactors of MAB21L2 using a yeast two-hybrid screen followed by additional validations in both yeast and human cells.

Several interactions were identified in three independent MAB21L2/mab21l2 wild-type screens with high confidence scores. These included TNPO2/tnpo2/tnpo1, KLC2/klc2, SPTBN1/sptbn1 and klhl31. The identification of tnpo1 and TNPO2/tnpo2, with both transportins participating as nuclear transport receptors for nuclear import [28,29], is consistent with previous data showing MAB21L2 is localized primarily to the nucleus [2,12]. KLC2 [30] and SPTBN1 [19] have been associated with TGF-β signaling; MAB21L2 likewise has been implicated in this pathway [13,14]. Finally, Klhl31, a kelch-like family member, has been found to modulate canonical WNT signaling [31] and act as a repressor in MAPK/JNK

signaling [32], of which both pathways have been implicated in eye development [33–35]. To note, these interactions were observed with high confidence for both wild-type and mutant (p.Arg51Gly) MAB21L2 proteins, indicating that they are not affected by the human disease-associated variant. If transportins are involved in MAB21L2 nuclear import, this would be consistent with previous reports that nuclear localization is uninterrupted for MAB21L2-p.(Arg51Gly) [2].

Through the yeast two-hybrid assays, we also revealed interactions that were potentially unique to or favored by the MAB21L2-p.(Arg51Gly) mutant in comparison to the wild-type protein. This discovered high confidence interactions with hspa5 and hspa8, two different heat shock proteins. *HSPA5* and *HSPA8* genes encode for HSP70 proteins, with *HSPA5* encoding for an endoplasmic reticulum-specific HSP70, otherwise known as BiP or GRP-78, and *HSPA8* encoding constitutively active HSP70 (HSC70).

*HSPA5* encoded GRP-78 (Bip) is known for its role in maintenance of proteostasis, specifically within the endoplasmic reticulum [36–38]. It has a major role in regulation of the unfolded protein response (UPR) [36–38]. However, it has also been found in several additional compartments throughout the cell. Reports have identified GRP-78 at the plasma membrane where it acts as a co-receptor in signal transduction [39–41]. Additional studies have also confirmed the presence of HSPA5 in the nucleus of human cells [20,22]. In mice, *Hspa5* null animals demonstrate early embryonic lethality, while heterozygotes develop without any obvious abnormalities [42]. Another study demonstrated an important role for *Hspa5* in kidney development in *Xenopus laevis* via regulation of retinoic acid signaling [22]. Retinoic acid (RA) signaling is also a pathway with known importance in ocular development [43], and several RA pathway genes have been implicated in MAC-spectrum disease, including *STRA6* [44–51] *ALDH1A3* [52], *RARB* [52–54] and *RBP4* [55–57].

HSC70, encoded by *HSPA8*, is most well-known for its classical role as a molecular chaperone where it participates in the maintenance of proteostasis (via assisting protein folding, translocation, assembly/disassembly of complexes, and degradation) [58]. Additionally, it is also known to be located throughout the cell in various compartments, including the nucleus, MAB21L2's primary subcellular compartment [2,12]. Previous work has shown an ability for HSC70 proteins to shuttle across the nuclear envelope [59] and import other cytosolic proteins with nuclear localization signals (NLS) [60]. The *HSPA8* gene also contains two of its own NLS's [21,23]. Interestingly, previous work has also shown that in response to a stress stimuli, HSC70 nucleocytoplasmic shuttling becomes inhibited and the protein remains sequestered in the nucleus [61]. Additionally, it has been demonstrated that if HSC70 is prohibited from nuclear release during the recovery phase post-stress, cell survival is negatively affected upon application of a secondary stressor event [62], suggesting it's shuttling capability is vital. Finally, there have been various reports implicating Hspa8 (Hsc70) in transcriptional regulation and involvement in assembly of complexes at promoter regions [63–65].

The interaction of MAB21L2 wild-type and p.(Arg51Gly) mutant proteins with HSPA5/hspa5 and HSPA8/hspa8 was validated by mass spectrometry, 1-by-1 assay (for zebrafish hspa8), as well as co-IP experiments in HLE-B3 cells (for both HSPA5 and HSPA8),

thus confirming them as novel interacting partners of MAB21L2. Contrary to the results from Y2H, where hspa8 and hspa5 were unique interactions specific to the MAB21L2 p.(Arg51Gly) mutant, other assays demonstrated that both wild-type and mutant MAB21L2 proteins are able to interact with these heat shock proteins; of note, trends towards a weaker interaction for the wild-type were evident in two of the validation assays but with no statistically significant difference. While a difference in protein-binding affinity remains a possibility, other methods for its quantification will need to be employed in order to clarify this issue. Overall, a stronger association of HSPA8 with the MAB21L2 p.(Arg51Gly) mutant would be consistent with its role in facilitating correct protein folding, as well as stabilizing or degrading mutant proteins.

Neither *HSPA5* nor *HSPA8* are currently associated with distinct human phenotypes. Studies of a zebrafish *hspa8* mutant, $hspa8^{hi138Tg}$, demonstrated its importance in normal embryonic development, including the eye. Ocular and systemic phenotypes were present at all examined stages; the ocular phenotype was severe and included small, underdeveloped eyes, with abnormal retina morphology, coloboma and anterior segment (lens and corneal) defects. These features overlap phenotypes observed in *mab21l2*-deficient lines [2,66–68]. Moreover, embryos with double deficiency for $hspa8^{hi138Tg}$ and $mab21l2^{Arg51\_Phe52del}$ ($mab21l2^{mw702}$) demonstrated more pronounced phenotypes suggesting functional interaction between these factors: fish with homozygosity for *hspa8* in *mab21l2* heterozygous background showed stronger coloboma phenotypes than *hspa8* homozygotes with wild-type *mab21l2* alleles while embryos with *mab21l2* homozygosity in *hspa8* heterozygous background showed a significant reduction in lens size in comparison to single *mab21l2* homozygotes; double homozygous embryos displayed the most severe phenotypes with the highest grade/incidence of coloboma and smallest lenses. This indicates a possible role for HSPA8/hspa8 in stabilization and correct folding of wild-type and mutant MAB21L2/mab21l2 proteins, supported by more severe disease in the $mab21l2^{Arg51\_Phe52del}$ mutant in *hspa8*-deficient background. Furthermore, these data suggest a possible role of *HSPA5* and/or *HSPA8* variants in the phenotypic variability associated with *MAB21L2* alleles in human families that needs to be investigated.

## Experimental Procedures

### Yeast Two-Hybrid (Y2H) Screen and Interaction Confirmation

A full-length N-terminal tagged human *MAB21L2* (NM_006439) wild-type (#EX-V1703-M11, Genecopoeia, Rockville, MD, USA) and a mutant human *MAB21L2*-p.(Arg51Gly) (all in a pEZ-M11 vector), previously described[2], as well as zebrafish mab21l2 were used in Y2H analysis [2].

All plasmids were submitted to Hybrigenics Services (https://www.hybrigenics-services.com/; Evry, France) for use in the ULTImate Y2H™ screening analysis which was conducted as previously described [69]. Briefly, in the initial set of screens, human *MAB21L2* and *MAB21L2*-p.(Arg51Gly) cDNA were cloned into a pB66 [69] vector to be expressed in-frame with a N-terminal GAL4 DNA binding domain. Constructs were tested for autoactivation of the *HIS3* gene reporter and treated with 3-aminotriazol (3AT) if needed. The following prey libraries were tested: MAB21L2-WT vs. human retina, MAB21L2-WT

vs. zebrafish embryo (18-20 hours post fertilization (hpf)) and MAB21L2-p.(Arg51Gly) vs. zebrafish embryo (18-20 hpf). In a second set of screens, zebrafish (*Danio rerio*) *mab21l2* cDNA was cloned into both a pB27, (derived from pBTM116 [70]), to be expressed in-frame with a N-terminal LexA binding domain, and the pB66 vector, as described above. Both were screened against a zebrafish embryo (18-20 hpf) prey library.

Data was analyzed and each identified interaction was assigned a Predicted Biological Score (PBS®), a statistically calculated confidence score [71,72]. Briefly, confidence scores were classified as follows: A- Very high confidence, B- High confidence, C- Good confidence, D- Moderate confidence (includes likely false-positives or interactions with low mRNA representation in prey library), E-unreliable due to non-specific interactions, F- technical artifacts.

To test individual interactions in yeast, a 1-by-1 assay was also conducted through Hybrigenics Services, which is based on the reconstitution of an active transcription factor to initiate expression of a *HIS3* gene reporter. Briefly, full-length bait proteins (MAB21L2-WT or MAB21L2-p.(Arg51Gly), as used in the initial Y2H screen above) were cloned in frame into pB66 [69], to be expressed as a C-terminal fusion to a GAL4 DNA binding domain. The prey fragment for hspa8 was extracted from the ULTImate Y2H™ screen (specifically, MAB21L2-p.(Arg51Gly) against the Zebrafish Embryo (18-20 hpf) library) and was cloned into a pP6 plasmid [73] to be expressed in frame with a GAL4 activation domain. The assay was conducted by transforming bait constructs into yeast haploid cells CG945 (mata) and prey constructs into YHGX13 (Y187 ade20101::loxP-kanMX-loxP, mata). Yeast cells were mated to obtain diploids [69]. To note, SMAD and SMURF were used as control bait and prey constructs, respectively [74]. Yeast cells were grown on two different selective mediums. DO-2 lacks tryptophan and leucine and was used as a control to determine that both bait and prey were present; DO-3 lacks tryptophan, leucine and histidine, where growth in the absence of histidine suggests an interaction between the bait and prey.

## Co-Immunoprecipitation (co-IP) studies

HSPA8 and HSPA5 interactions with MAB21L2 were tested using co-IP. Briefly, human lens epithelial (HLE-B3) cells (CRL-11421™, ATCC®, Manassas, VA, USA) were transfected with 7.5ug of bait (N-terminal FLAG-tagged MAB21L2 or MAB21L2-p.(Arg51Gly), described above) and 7.5ug prey. HLE-B3 cells demonstrate endogenous expression of *MAB21L2*[2]. Prey constructs were as follows: Full-length C-terminal Myc tagged HSPA8 (NM_006597; #EX-W1208-M09, GeneCopoeia) and HSPA5 (NM_005347; #EX-T3592-M09, GeneCopoeia) in a pEZ-M09 vector or control Invitrogen™ pcDNA3.1 vector (V79020, ThermoFisher Scientific, Waltham, MA, USA). Transfections were conducted using Invitrogen™ Lipofectamine™ 2000 Transfection Reagent (11668019, ThermoFisher Scientific) with Opti-MEM (31985070, ThermoFisher Scientific). Cells were cultured as previously described [8]. Two methods were used for co-IP: 1) whole-cell lysates were collected 48 hours post transfection and lysed with 1% Triton X-100 (with protease inhibitor and phosphatase inhibitor). An aliquot was reserved for input control. Then, lysates were incubated with a monoclonal anti-FLAG M2 antibody produced in mouse (F1804-200UG, Sigma Aldrich) rotating overnight at 4°C. Following, the antibody-

lysate sample was incubated with protein A/G PLUS-Agarose beads (sc-2003, Santa Cruz Biotechnology, Inc., Dallas, TX, USA) rotating 2 hours at 4°C. Beads were washed with 1% Triton X-100 and proteins eluted from beads with 1X sample buffer and heating at 95°C for 5 minutes. 2) whole-cell lysates were collected 48 hours post-transfection and lysed with a 1X immunoprecipitation (IP) Buffer (1% Triton X-100, 150 mM NaCl, 20mM Tris-HCl pH7.5, 1mM EDTA). An aliquot was reserved for input control. Lysates were incubated with Anti-FLAG® M2 Magnetic Beads (#M8823, Sigma-Aldrich, St. Louis, MO, USA) overnight at 4°C. The Beads were washed with 1X IP buffer and protein was eluted from beads via incubation with 4X Laemmli buffer at 50°C for 10 minutes. Western blot was conducted using a wet-tank transfer and membrane probed. The following antibodies were utilized: 1:1000 Myc-Tag (9B11) Mouse mAb (#2276S, Cell Signaling, Danvers, MA, USA), monoclonal mouse anti-FLAG (F1804-200UG, Sigma Aldrich), Myc-Tag (71D10) Rabbit mAb (#2278, Cell Signaling Technology) and polyclonal rabbit anti-FLAG (SAB1306078-400UL, Sigma-Aldrich) primary antibodies; 1:2000 goat anti-mouse (#PA1-74421, ThermoFisher Scientific) and goat anti-rabbit (#32460, ThermoFisher Scientific) HRP conjugated secondary antibodies.

## Mass Spectrometry

HLE-B3 cells were transfected with 7.5μg of N-terminally FLAG-tagged MAB21L2 wild-type or MAB21L2-p.(Arg51Gly), as described above. Two days post-transfection cells were collected and incubated in lysis buffer (50mM HEPES pH7.4, 150mM NaCl, 150mM egtazic acid (EGTA), 10% glycerol, 1% Triton X-100) for 30 minutes on ice. Then, cells were spun down (12,000 X g, 10 minutes, 4°C) and the supernatant collected. Cell lysate was then incubated overnight at 4°C with monoclonal mouse anti-FLAG (F1804-200UG, Sigma Aldrich), phosphatase inhibitor and protease inhibitor. The following day, cell lysate mixture was incubated with Dynabeads™ Protein G (10003D, ThermoFisher Scientific) for 45 minutes at 4°C. Then, a series of washes were performed, 3 times with IP washing buffer (50mM HEPES pH7.5, 150mM NaCl, 1mM EGTA, 1.5mM MgCl2, 0.1% IgePal), and then twice with a no detergent IP buffer (50mM HEPES, 150mM NaCl, 1mM ethylenediaminetetraacetic acid (EDTA)). The samples were then submitted to the Medical College of Wisconsin Mass Spectrometry Core for analysis.

## Studies of zebrafish lines

The care and use of zebrafish (*Danio rerio*) was approved by the Institutional Animal Care and Use Committee at the Medical College of Wisconsin. Housing, care and breeding was carried out as previously described [75]. Age was determined by hours post fertilization (hpf) and days post fertilization (dpf), along with a morphological assessment [76].

The *hspa8*$^{hi138Tg}$ (transgenic insertion upstream of the *hspa8* coding region) zebrafish line was obtained from the Zebrafish International Resource Center (ZIRC) and used for characterization of the ocular phenotype. The line was generated using retroviral-mediated insertional mutagenesis [25] using previously established protocols for zebrafish [26]. The exact upstream position of the transgene to the *hspa8* start codon was determined using PCR to amplify a region containing the transgene and subsequent genomic region of *hspa8* (primers F-5'-CAAACCTACAGGTGGGGTCTTTC-3' anneals to retroviral insertion,

R-5'-GGGACTTCAACCGACAAGAACC-3' anneals to *hspa8* genomic region) followed by Sanger sequencing (primer R-5'-TGAATGAAATCACCCTGCAC-3'). Genotype was determined using two separate PCRs, 1) to determine the presence of the mutant allele (F-5'-CAAACCTACAGGTGGGGTCTTTC-3', R-5'-GGGACTTCAACCGACAAGAACC-3'; wild-type will have no amplification), 2) to determine the presence of wild-type allele and thus discriminate between heterozygous or homozygous *hspa8* mutants (F-5'-TCAAAAGCCATTCGTGATGA-3', R-5'-GGGACTTCAACCGACAAGAACC-3'; homozygotes will have no amplification).

To generate *hspa8*$^{hi138Tg}$/*mab21l2*-deficient double heterozygous fish, a previously generated heterozygous *mab21l2*$^{Arg51\_Phe52del}$ line (*mab21l2*$^{mw702}$ as catalogued in ZFIN (Zebrafish Information Network)) [2], was crossed with heterozygous *hspa8*$^{hi138Tg}$ fish. Embryos were raised to adulthood and genotyped, using the above protocol for *hspa8*, and as previously described for *mab21l2* [2].

Whole-mount images of 24, 48 and 72-hpf zebrafish were taken using a ZEISS SteREO Discovery.V12 microscope (Carl Zeiss Inc., Thornwood, NY, USA) with a ZEISS AxioCam MRc or AxioCam 305 Color (Carl Zeiss Inc.). Coloboma severity grading for 48-hpf *hspa8*$^{hi138Tg}$;*mab21l2*$^{Arg51\_Phe52del}$ embryos was performed blinded by two individuals for all genotype combinations using the grading protocol in Brown et al. (2009) as a guide, with modification for a 48-hpf timepoint [77]. For grade 0, a normal eye with a fully closed optic fissure was observed, for grade 1- no gap but a visible line likely indicating the presence of intact basement membrane was present, for grade 2- an obvious small gap between the opposing retinal margins was observed, for grade 3- a medium sized gap between the disorderly aligned retinal margins (equal or exceeding pupil radius in any part of the gap) was present, and for grade 4- a large gap between the disorderly aligned retinal margins (greater than pupil diameter in any part of the gap) was noted. Measurements of lens area were taken utilizing ImageJ software (https://imagej.nih.gov/ij/) by outlining the lens boundary three times and calculating an average area. All graphs were generated using GraphPad Prism 9 (San Diego, CA, USA' https://www.graphpad.com/scientific-software/prism/).

Histological analysis of 24-, 48- and 72-hpf wild-type and homozygous *hspa8*$^{hi138Tg}$ embryos and 24-hpf *hspa8*$^{hi138Tg}$;*mab21l2*$^{Arg51\_Phe52del}$ embryos, reared in either E2 embryo medium or 1X phenylthiourea, were performed as previously described [75], where embryos were fixed in Davidson's solution overnight and then transferred to 70% ethanol; preserved embryos were encapsulated in histogel (HG-4000-012, ThermoFisher Scientific) and submitted to the Medical College of Wisconsin Histology Core for processing, sectioning and H&E staining.

## In situ hybridization and qRT-PCR analyses

*In situ* hybridization was performed to determine the expression pattern of *hspa5* and *hspa8*, as previously described [75] using the following probes: Dr-mab21l2-C2 (499581-C2, Advanced Cell Diagnostics (ACD), Newark, CA, USA), Dr-hspa8-C3 (499661-C3, ACD), and Dr-hspa5-C3 (499651-C3, ACD).

For qRT-PCR analysis of *hspa8* transcript levels, two biological replicates (5 embryos each) of 48-hpf homozygous *hspa8*$^{hi138Tg}$ embryos were collected from a *hspa8*$^{hi138Tg/+}$ X *hspa8*$^{hi138Tg/+}$ cross. Tails were used for genotyping, and the heads/trunks processed for RNA. RNA was isolated using the Direct-zol™ RNA MiniPrep kit (R2052, ZymoResearch, Irvine, CA, USA). cDNA was synthesized using SuperScript III First Strand Synthesis System (18080051, ThermoFisher Scientific). Zebrafish *hspa8* and *actb1* were amplified from cDNA. For *hspa8* the following primer pairs were utilized: 1) F-5'-TTGATCTCGGGACCACCTAC-3' (exon 2), R-5'-TCAGACTGAACAACGCCATC-3' (exon 3) (210 base pairs (bp) intron between; expected product size 232 bp); 2) F-5'-TTGATCTCGGGACCACCTAC-3' (exon 2), R-5'-CAGCAGCAGTTGGTTCATTG (exon 4) (includes exon 3 and 2 introns (210bp and 212 bp); expected product size 513 bp). For *actb1*, the following primer pair was utilized: F-5′-GAGAAGATCTGGCATCACAC-3′ (exon 3), R-5′-ATCAGGTAGTCTGTCAGGTC-3′ (exon 4) (311 bp intron between; expected product size from cDNA 323 bp). qRT-PCR was then conducted where samples were run in triplicate and a no template control was included; fold change was calculated. Graphs were generated using GraphPad Prism 9. Statistical significance was determined using an unpaired sample t-test with a P value of $<0.05$.

## Supplementary Material

Refer to Web version on PubMed Central for supplementary material.

## Acknowledgments

This work was supported by National Institutes of Health grants R01EY025718 and T32EY014537 as well as funds provided by the Children's Research Institute Foundation at Children's Wisconsin (EVS) and National Institutes of Health awards R21EY25831 and P30 EY08098 (JMG).

## References

1. Aubert-Mucca M, Pernin-Grandjean J, Marchasson S, et al. Confirmation of FZD5 implication in a cohort of 50 patients with ocular coloboma. Eur J Hum Genet. Jul 31 2020. 10.1038/s41431-020-0695-8.
2. Deml B, Kariminejad A, Borujerdi RH, Muheisen S, Reis LM, Semina EV. Mutations in MAB21L2 result in ocular Coloboma, microcornea and cataracts. PLoS Genet. 2015;11(2):e1005002. 10.1371/journal.pgen.1005002. [PubMed: 25719200]
3. Horn D, Prescott T, Houge G, et al. A Novel Oculo-Skeletal syndrome with intellectual disability caused by a particular MAB21L2 mutation. Eur J Med Genet. Aug 2015;58(8):387–91. 10.1016/j.ejmg.2015.06.003. [PubMed: 26116559]
4. Patel N, Khan AO, Alsahli S, et al. Genetic investigation of 93 families with microphthalmia or posterior microphthalmos. Clin Genet. Jun 2018;93(6):1210–1222. 10.1111/cge.13239. [PubMed: 29450879]
5. Rainger J, Pehlivan D, Johansson S, et al. Monoallelic and biallelic mutations in MAB21L2 cause a spectrum of major eye malformations. Am J Hum Genet. Jun 5 2014;94(6):915–23. 10.1016/j.ajhg.2014.05.005. [PubMed: 24906020]
6. Bruel AL, Masurel-Paulet A, Riviere JB, et al. Autosomal recessive truncating MAB21L1 mutation associated with a syndromic scrotal agenesis. Clin Genet. Feb 2017;91(2):333–338. 10.1111/cge.12794. [PubMed: 27103078]
7. Rad A, Altunoglu U, Miller R, et al. MAB21L1 loss of function causes a syndromic neurodevelopmental disorder with distinctive cerebellar, ocular, craniofacial and genital features

(COFG syndrome). J Med Genet. May 2019;56(5):332–339. 10.1136/jmedgenet-2018-105623. [PubMed: 30487245]

8. Seese SE, Reis LM, Deml B, et al. Identification of missense MAB21L1 variants in microphthalmia and aniridia. Human Mutation 2021. 10.1002/humu.24218.
9. Ablasser A, Goldeck M, Cavlar T, et al. cGAS produces a 2′-5′-linked cyclic dinucleotide second messenger that activates STING. Nature. Jun 20 2013;498(7454):380–4. 10.1038/nature12306.
10. de Oliveira Mann CC, Kiefersauer R, Witte G, Hopfner KP. Structural and biochemical characterization of the cell fate determining nucleotidyltransferase fold protein MAB21L1. Sci Rep. Jun 8 2016;6:27498. 10.1038/srep27498.
11. Gao P, Ascano M, Wu Y, et al. Cyclic [G(2′,5′)pA(3′,5′)p] is the metazoan second messenger produced by DNA-activated cyclic GMP-AMP synthase. Cell. May 23 2013;153(5):1094–107. 10.1016/j.cell.2013.04.046. [PubMed: 23647843]
12. Mariani M, Baldessari D, Francisconi S, et al. Two murine and human homologs of mab-21, a cell fate determination gene involved in Caenorhabditis elegans neural development. Hum Mol Genet. Dec 1999;8(13):2397–406. 10.1093/hmg/8.13.2397. [PubMed: 10556287]
13. Baldessari D, Badaloni A, Longhi R, Zappavigna V, Consalez GG. MAB21L2, a vertebrate member of the Male-abnormal 21 family, modulates BMP signaling and interacts with SMAD1. BMC Cell Biol. Dec 21 2004;5(1):48. 10.1186/1471-2121-5-48. [PubMed: 15613244]
14. Morita K, Chow KL, Ueno N. Regulation of body length and male tail ray pattern formation of Caenorhabditis elegans by a member of TGF-beta family. Development. Mar 1999;126(6):1337–47. [PubMed: 10021351]
15. Baird SE, Fitch DH, Kassem IA, Emmons SW. Pattern formation in the nematode epidermis: determination of the arrangement of peripheral sense organs in the C. elegans male tail. Development. Oct 1991;113(2):515–26. [PubMed: 1782863]
16. St-Onge L, Sosa-Pineda B, Chowdhury K, Mansouri A, Gruss P. Pax6 is required for differentiation of glucagon-producing alpha-cells in mouse pancreas. Nature. May 22 1997;387(6631):406–9. 10.1038/387406a0. [PubMed: 9163426]
17. Wolf LV, Yang Y, Wang J, et al. Identification of pax6-dependent gene regulatory networks in the mouse lens. PLoS One. 2009;4(1):e4159. 10.1371/journal.pone.0004159. [PubMed: 19132093]
18. Yamada R, Mizutani-Koseki Y, Hasegawa T, Osumi N, Koseki H, Takahashi N. Cell-autonomous involvement of Mab21l1 is essential for lens placode development. Development. May 2003;130(9):1759–70. 10.1242/dev.00399. [PubMed: 12642482]
19. Tang Y, Katuri V, Dillner A, Mishra B, Deng CX, Mishra L. Disruption of transforming growth factor-beta signaling in ELF beta-spectrin-deficient mice. Science. Jan 24 2003;299(5606):574–7. 10.1126/science.1075994. [PubMed: 12543979]
20. Bellucci A, Navarria L, Zaltieri M, et al. Induction of the unfolded protein response by alpha-synuclein in experimental models of Parkinson's disease. J Neurochem. Feb 2011;116(4):588–605. 10.1111/j.1471-4159.2010.07143.x. [PubMed: 21166675]
21. Lamian V, Small GM, Feldherr CM. Evidence for the existence of a novel mechanism for the nuclear import of Hsc70. Exp Cell Res. Oct 10 1996;228(1):84–91. 10.1006/excr.1996.0302. [PubMed: 8892974]
22. Shi W, Xu G, Wang C, et al. Heat shock 70-kDa protein 5 (Hspa5) is essential for pronephros formation by mediating retinoic acid signaling. J Biol Chem. Jan 2 2015;290(1):577–89. 10.1074/jbc.M114.591628. [PubMed: 25398881]
23. Tsukahara F, Maru Y. Identification of novel nuclear export and nuclear localization-related signals in human heat shock cognate protein 70. J Biol Chem. Mar 5 2004;279(10):8867–72. 10.1074/jbc.M308848200. [PubMed: 14684748]
24. Bonam SR, Ruff M, Muller S. HSPA8/HSC70 in Immune Disorders: A Molecular Rheostat that Adjusts Chaperone-Mediated Autophagy Substrates. Cells. Aug 7 2019;8(8). 10.3390/cells8080849.
25. Amsterdam A, Nissen RM, Sun Z, Swindell EC, Farrington S, Hopkins N. Identification of 315 genes essential for early zebrafish development. Proc Natl Acad Sci U S A. Aug 31 2004;101(35):12792–7. 10.1073/pnas.0403929101. [PubMed: 15256591]

26. Amsterdam A, Burgess S, Golling G, et al. A large-scale insertional mutagenesis screen in zebrafish. Genes Dev. Oct 15 1999;13(20):2713–24. 10.1101/gad.13.20.2713. [PubMed: 10541557]
27. Gross JM, Perkins BD, Amsterdam A, et al. Identification of zebrafish insertional mutants with defects in visual system development and function. Genetics. May 2005;170(1):245–61. 10.1534/genetics.104.039727. [PubMed: 15716491]
28. Fridell RA, Truant R, Thorne L, Benson RE, Cullen BR. Nuclear import of hnRNP A1 is mediated by a novel cellular cofactor related to karyopherin-beta. J Cell Sci. Jun 1997;110 ( Pt 11):1325–31. [PubMed: 9202393]
29. Siomi MC, Eder PS, Kataoka N, Wan L, Liu Q, Dreyfuss G. Transportin-mediated nuclear import of heterogeneous nuclear RNP proteins. J Cell Biol. Sep 22 1997;138(6):1181–92. 10.1083/jcb.138.6.1181. [PubMed: 9298975]
30. Batut J, Howell M, Hill CS. Kinesin-mediated transport of Smad2 is required for signaling in response to TGF-beta ligands. Dev Cell. Feb 2007;12(2):261–74. 10.1016/j.devcel.2007.01.010.
31. Abou-Elhamd A, Alrefaei AF, Mok GF, et al. Klhl31 attenuates beta-catenin dependent Wnt signaling and regulates embryo myogenesis. Dev Biol. Jun 1 2015;402(1):61–71. 10.1016/j.ydbio.2015.02.024. [PubMed: 25796573]
32. Yu W, Li Y, Zhou X, et al. A novel human BTB-kelch protein KLHL31, strongly expressed in muscle and heart, inhibits transcriptional activities of TRE and SRE. Mol Cells. Nov 30 2008;26(5):443–53. [PubMed: 18719355]
33. Fuhrmann S. Wnt signaling in eye organogenesis. Organogenesis. Apr 2008;4(2):60–7. 10.4161/org.4.2.5850. [PubMed: 19122781]
34. Syc-Mazurek SB, Rausch RL, Fernandes KA, Wilson MP, Libby RT. Mkk4 and Mkk7 are important for retinal development and axonal injury-induced retinal ganglion cell death. Cell Death Dis. Oct 26 2018;9(11):1095. 10.1038/s41419-018-1079-7. [PubMed: 30367030]
35. Weston CR, Wong A, Hall JP, Goad ME, Flavell RA, Davis RJ. JNK initiates a cytokine cascade that causes Pax2 expression and closure of the optic fissure. Genes Dev. May 15 2003;17(10):1271–80. 10.1101/gad.1087303. [PubMed: 12756228]
36. Hendershot LM. The ER function BiP is a master regulator of ER function. Mt Sinai J Med. Oct 2004;71(5):289–97. [PubMed: 15543429]
37. Lee AS. The ER chaperone and signaling regulator GRP78/BiP as a monitor of endoplasmic reticulum stress. Methods. Apr 2005;35(4):373–81. 10.1016/j.ymeth.2004.10.010. [PubMed: 15804610]
38. Wang M, Wey S, Zhang Y, Ye R, Lee AS. Role of the unfolded protein response regulator GRP78/BiP in development, cancer, and neurological disorders. Antioxid Redox Signal. Sep 2009;11(9):2307–16. 10.1089/ARS.2009.2485. [PubMed: 19309259]
39. Al-Hashimi AA, Caldwell J, Gonzalez-Gronow M, et al. Binding of anti-GRP78 autoantibodies to cell surface GRP78 increases tissue factor procoagulant activity via the release of calcium from endoplasmic reticulum stores. J Biol Chem. Sep 10 2010;285(37):28912–23. 10.1074/jbc.M110.119107. [PubMed: 20605795]
40. Shani G, Fischer WH, Justice NJ, Kelber JA, Vale W, Gray PC. GRP78 and Cripto form a complex at the cell surface and collaborate to inhibit transforming growth factor beta signaling and enhance cell growth. Mol Cell Biol. Jan 2008;28(2):666–77. 10.1128/MCB.01716-07. [PubMed: 17991893]
41. Zhang Y, Liu R, Ni M, Gill P, Lee AS. Cell surface relocalization of the endoplasmic reticulum chaperone and unfolded protein response regulator GRP78/BiP. J Biol Chem. May 14 2010;285(20):15065–75. 10.1074/jbc.M109.087445. [PubMed: 20208072]
42. Luo S, Mao C, Lee B, Lee AS. GRP78/BiP is required for cell proliferation and protecting the inner cell mass from apoptosis during early mouse embryonic development. Mol Cell Biol. Aug 2006;26(15):5688–97. 10.1128/MCB.00779-06. [PubMed: 16847323]
43. Cvekl A, Wang WL. Retinoic acid signaling in mammalian eye development. Exp Eye Res. Sep 2009;89(3):280–91. 10.1016/j.exer.2009.04.012. [PubMed: 19427305]

44. Casey J, Kawaguchi R, Morrissey M, et al. First implication of STRA6 mutations in isolated anophthalmia, microphthalmia, and coloboma: a new dimension to the STRA6 phenotype. Hum Mutat. Dec 2011;32(12):1417–26. 10.1002/humu.21590. [PubMed: 21901792]
45. Chassaing N, Golzio C, Odent S, et al. Phenotypic spectrum of STRA6 mutations: from Matthew-Wood syndrome to non-lethal anophthalmia. Hum Mutat. May 2009;30(5):E673–81. 10.1002/humu.21023. [PubMed: 19309693]
46. Chassaing N, Ragge N, Kariminejad A, et al. Mutation analysis of the STRA6 gene in isolated and non-isolated anophthalmia/microphthalmia. Clin Genet. Mar 2013;83(3):244–50. 10.1111/j.1399-0004.2012.01904.x. [PubMed: 22686418]
47. Chitayat D, Sroka H, Keating S, et al. The PDAC syndrome (pulmonary hypoplasia/agenesis, diaphragmatic hernia/eventration, anophthalmia/microphthalmia, and cardiac defect) (Spear syndrome, Matthew-Wood syndrome): report of eight cases including a living child and further evidence for autosomal recessive inheritance. Am J Med Genet A. Jun 15 2007;143A(12):1268–81. 10.1002/ajmg.a.31788. [PubMed: 17506106]
48. Golzio C, Martinovic-Bouriel J, Thomas S, et al. Matthew-Wood syndrome is caused by truncating mutations in the retinol-binding protein receptor gene STRA6. Am J Hum Genet. Jun 2007;80(6):1179–87. 10.1086/518177. [PubMed: 17503335]
49. Ng WY, Pasutto F, Bardakjian TM, et al. A puzzle over several decades: eye anomalies with FRAS1 and STRA6 mutations in the same family. Clin Genet. Feb 2013;83(2):162–8. 10.1111/j.1399-0004.2012.01851.x. [PubMed: 22283518]
50. Pasutto F, Sticht H, Hammersen G, et al. Mutations in STRA6 cause a broad spectrum of malformations including anophthalmia, congenital heart defects, diaphragmatic hernia, alveolar capillary dysplasia, lung hypoplasia, and mental retardation. Am J Hum Genet. Mar 2007;80(3):550–60. 10.1086/512203. [PubMed: 17273977]
51. Seller MJ, Davis TB, Fear CN, Flinter FA, Ellis I, Gibson AG. Two sibs with anophthalmia and pulmonary hypoplasia (the Matthew-Wood syndrome). Am J Med Genet. Mar 29 1996;62(3):227–29. 10.1002/(SICI)1096-8628(19960329)62:3<227::AID-AJMG5>3.0.CO;2-Q. [PubMed: 8882778]
52. Fares-Taie L, Gerber S, Chassaing N, et al. ALDH1A3 mutations cause recessive anophthalmia and microphthalmia. Am J Hum Genet. Feb 7 2013;92(2):265–70. 10.1016/j.ajhg.2012.12.003. [PubMed: 23312594]
53. Srour M, Caron V, Pearson T, et al. Gain-of-Function Mutations in RARB Cause Intellectual Disability with Progressive Motor Impairment. Hum Mutat. Aug 2016;37(8):786–93. 10.1002/humu.23004. [PubMed: 27120018]
54. Srour M, Chitayat D, Caron V, et al. Recessive and dominant mutations in retinoic acid receptor beta in cases with microphthalmia and diaphragmatic hernia. Am J Hum Genet. Oct 3 2013;93(4):765–72. 10.1016/j.ajhg.2013.08.014. [PubMed: 24075189]
55. Chou CM, Nelson C, Tarle SA, et al. Biochemical Basis for Dominant Inheritance, Variable Penetrance, and Maternal Effects in RBP4 Congenital Eye Disease. Cell. Apr 23 2015;161(3):634–646. 10.1016/j.cell.2015.03.006. [PubMed: 25910211]
56. Cukras C, Gaasterland T, Lee P, et al. Exome analysis identified a novel mutation in the RBP4 gene in a consanguineous pedigree with retinal dystrophy and developmental abnormalities. PLoS One. 2012;7(11):e50205. 10.1371/journal.pone.0050205. [PubMed: 23189188]
57. Seeliger MW, Biesalski HK, Wissinger B, et al. Phenotype in retinol deficiency due to a hereditary defect in retinol binding protein synthesis. Invest Ophthalmol Vis Sci. Jan 1999;40(1):3–11. [PubMed: 9888420]
58. Liu T, Daniels CK, Cao S. Comprehensive review on the HSC70 functions, interactions with related molecules and involvement in clinical diseases and therapeutic potential. Pharmacol Ther. Dec 2012;136(3):354–74. 10.1016/j.pharmthera.2012.08.014. [PubMed: 22960394]
59. Mandell RB, Feldherr CM. Identification of two HSP70-related Xenopus oocyte proteins that are capable of recycling across the nuclear envelope. J Cell Biol. Nov 1990;111(5 Pt 1):1775–83. 10.1083/jcb.111.5.1775. [PubMed: 2229173]

60. Imamoto N, Matsuoka Y, Kurihara T, et al. Antibodies against 70-kD heat shock cognate protein inhibit mediated nuclear import of karyophilic proteins. J Cell Biol. Dec 1992;119(5):1047–61. 10.1083/jcb.119.5.1047. [PubMed: 1332978]
61. Kodiha M, Chu A, Lazrak O, Stochaj U. Stress inhibits nucleocytoplasmic shuttling of heat shock protein hsc70. Am J Physiol Cell Physiol. Oct 2005;289(4):C1034–41. 10.1152/ajpcell.00590.2004. [PubMed: 15930140]
62. Wang F, Bonam SR, Schall N, et al. Blocking nuclear export of HSPA8 after heat shock stress severely alters cell survival. Sci Rep. Nov 14 2018;8(1):16820. 10.1038/s41598-018-34887-6. [PubMed: 30429537]
63. Carter DA. Modulation of cellular AP-1 DNA binding activity by heat shock proteins. FEBS Lett. Oct 13 1997;416(1):81–5. 10.1016/s0014-5793(97)01174-5. [PubMed: 9369238]
64. Geng Y, Zhao Y, Schuster LC, et al. A Chemical Biology Study of Human Pluripotent Stem Cells Unveils HSPA8 as a Key Regulator of Pluripotency. Stem Cell Reports. Dec 8 2015;5(6):1143–1154. 10.1016/j.stemcr.2015.09.023. [PubMed: 26549849]
65. Yahata T, de Caestecker MP, Lechleider RJ, et al. The MSG1 non-DNA-binding transactivator binds to the p300/CBP coactivators, enhancing their functional link to the Smad transcription factors. J Biol Chem. Mar 24 2000;275(12):8825–34. 10.1074/jbc.275.12.8825. [PubMed: 10722728]
66. Gath N, Gross JM. Zebrafish mab21l2 mutants possess severe defects in optic cup morphogenesis, lens and cornea development. Dev Dyn. Jul 2019;248(7):514–529. 10.1002/dvdy.44. [PubMed: 31037784]
67. Hartsock A, Lee C, Arnold V, Gross JM. In vivo analysis of hyaloid vasculature morphogenesis in zebrafish: A role for the lens in maturation and maintenance of the hyaloid. Dev Biol. Oct 15 2014;394(2):327–39. 10.1016/j.ydbio.2014.07.024. [PubMed: 25127995]
68. Wycliffe R, Plaisancie J, Leaman S, et al. Developmental delay during eye morphogenesis underlies optic cup and neurogenesis defects in mab21l2u517 zebrafish mutants. Int J Dev Biol. Aug 26 2020. 10.1387/ijdb.200173lv.
69. Fromont-Racine M, Rain JC, Legrain P. Toward a functional analysis of the yeast genome through exhaustive two-hybrid screens. Nat Genet. Jul 1997;16(3):277–82. 10.1038/ng0797-277. [PubMed: 9207794]
70. Vojtek AB, Hollenberg SM. Ras-Raf interaction: two-hybrid analysis. Methods Enzymol. 1995;255:331–42. 10.1016/s0076-6879(95)55036-4. [PubMed: 8524119]
71. Formstecher E, Aresta S, Collura V, et al. Protein interaction mapping: a Drosophila case study. Genome Res. Mar 2005;15(3):376–84. 10.1101/gr.2659105. [PubMed: 15710747]
72. Rain JC, Selig L, De Reuse H, et al. The protein-protein interaction map of Helicobacter pylori. Nature. Jan 11 2001;409(6817):211–5. 10.1038/35051615. [PubMed: 11196647]
73. Bartel PL, Chein CT, Stemglanz R, Fields S. In: Hartley DA, ed. Cellular interactions in development: A practical approach. Oxford: Oxford University Press; 1993:153–179.
74. Colland F, Jacq X, Trouplin V, et al. Functional proteomics mapping of a human signaling pathway. Genome Res. Jul 2004;14(7):1324–32. 10.1101/gr.2334104. [PubMed: 15231748]
75. Seese SE, Deml B, Muheisen S, Sorokina E, Semina EV. Genetic disruption of zebrafish mab21l1 reveals a conserved role in eye development and affected pathways. Dev Dyn. Feb 11 2021. 10.1002/dvdy.312.
76. Kimmel CB, Ballard WW, Kimmel SR, Ullmann B, Schilling TF. Stages of embryonic development of the zebrafish. Dev Dyn. Jul 1995;203(3):253–310. 10.1002/aja.1002030302. [PubMed: 8589427]
77. Brown JD, Dutta S, Bharti K, et al. Expression profiling during ocular development identifies 2 Nlz genes with a critical role in optic fissure closure. Proc Natl Acad Sci U S A. Feb 3 2009;106(5):1462–7. 10.1073/pnas.0812017106. [PubMed: 19171890]

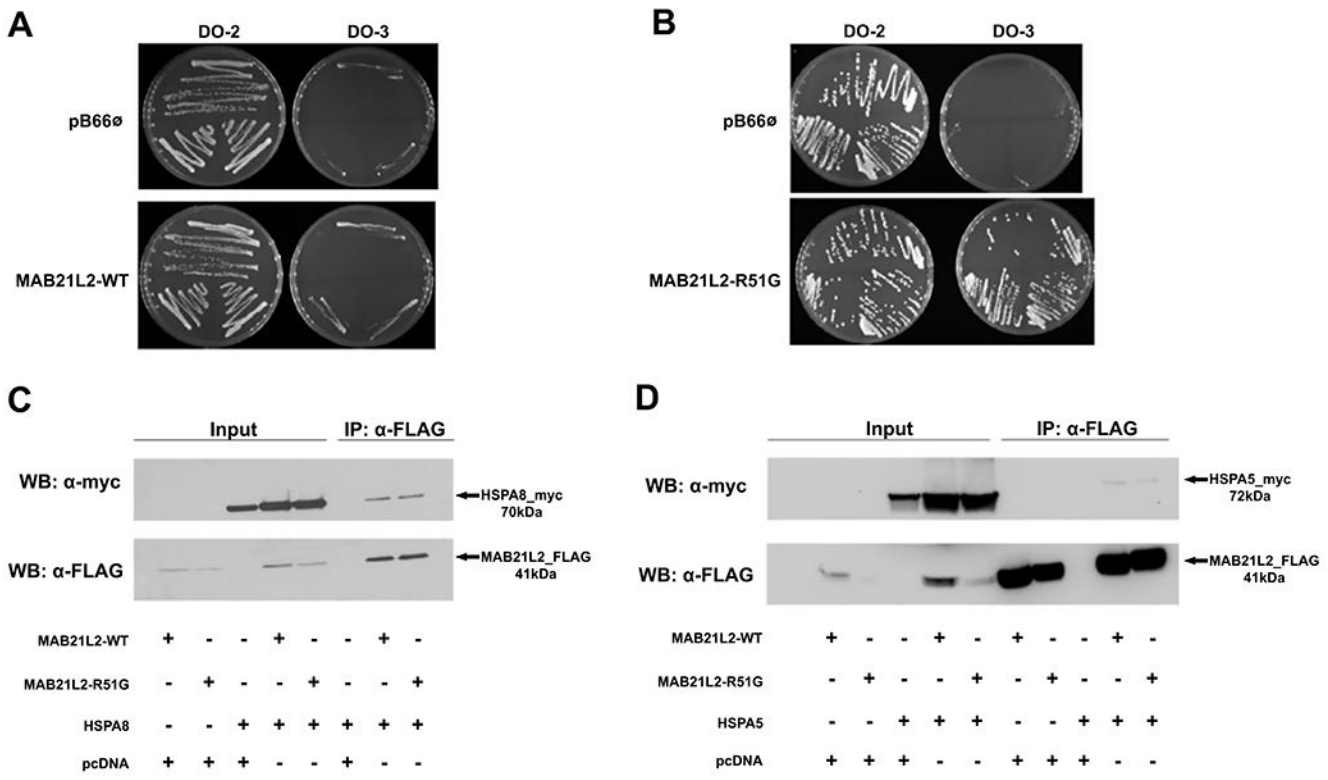


**Figure 1: HSPA8/HSPA5 interaction with MAB21L2 proteins.**

**A, B**. Growth plates for 1-by-1 Y2H interaction assay. pB66ø (empty GAL4 DNA-Binding Domain (DBD) vector) was used as a negative control. MAB21L2-WT (**A**) or MAB21L2-p.(Arg51Gly) (**B**) was tested against a zebrafish hspa8 fragment; yeast was grown on DO-2 (-tryptophan, -leucine; selects for presence of both bait and prey) and DO-3 selective media (-tryptophan, -leucine, -histidine; selects for interaction of bait and prey). Note the weakened yeast growth on DO-3 medium for MAB21L2-WT (**A**), in comparison to MAB21L2-p.(Arg51Gly) (**B**). **C, D**. Co-immunoprecipitation assay for human full-length FLAG-tagged MAB21L2-WT or MAB21L2-p.(Arg51Gly) and human full length myc-tagged HSPA8 (**C**) or HSPA5 (**D**). Cells were transfected with respective constructs, pcDNA empty plasmid was used as a control. Cell lysates were collected, with a portion reserved for 'input', and a portion immunoprecipitated with anti-FLAG antibodies. Western blot analysis with anti-myc antibodies for detection of HSPA8/5 and anti-FLAG antibodies for detection of MAB21L2-WT/p.(Arg51Gly) was performed. Both MAB21L2-WT and MAB21L2-p.(Arg51Gly) co-precipitated with HSPA8 and HSPA5.

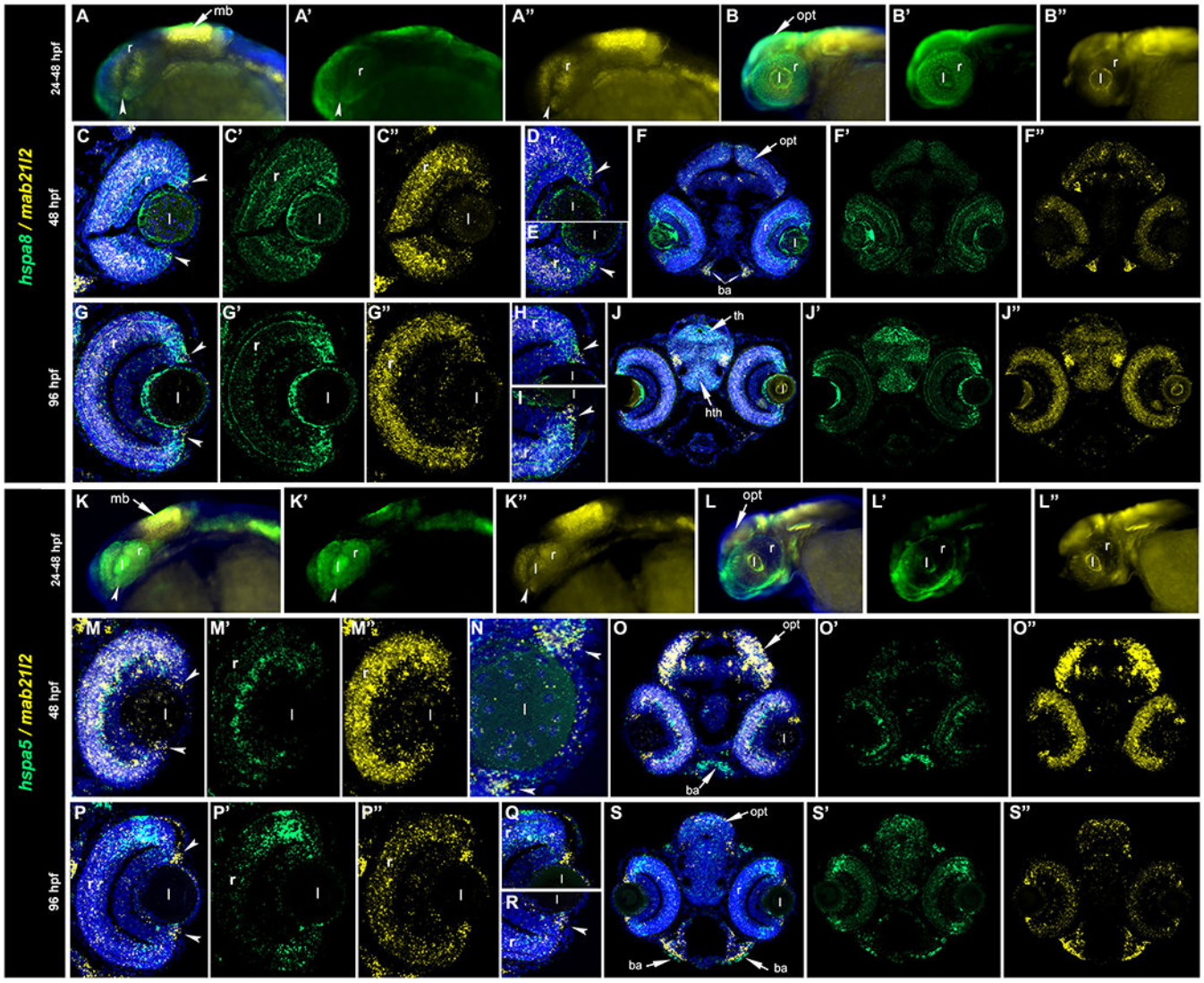


**Figure 2: Expression pattern of both *hspa5* and *hspa8* overlaps with *mab21l2* at embryonic stages.**

RNA-scope analysis of *hspa5* or *hspa8* (green) and *mab21l2* (yellow) in 24 (A-A" and K-K"), 48-(B-F" and L-O") and 96-hpf (G-J" and P-S") wild-type embryos. (l) lens, (r) retina, (mb) midbrain, (opt) optic tectum, (ba) branchial arches, (th) thalamus, (hth) hypothalamus. White arrows indicate the optic fissure (A-B, K-K") and ciliary marginal zone (C-I and M-R).

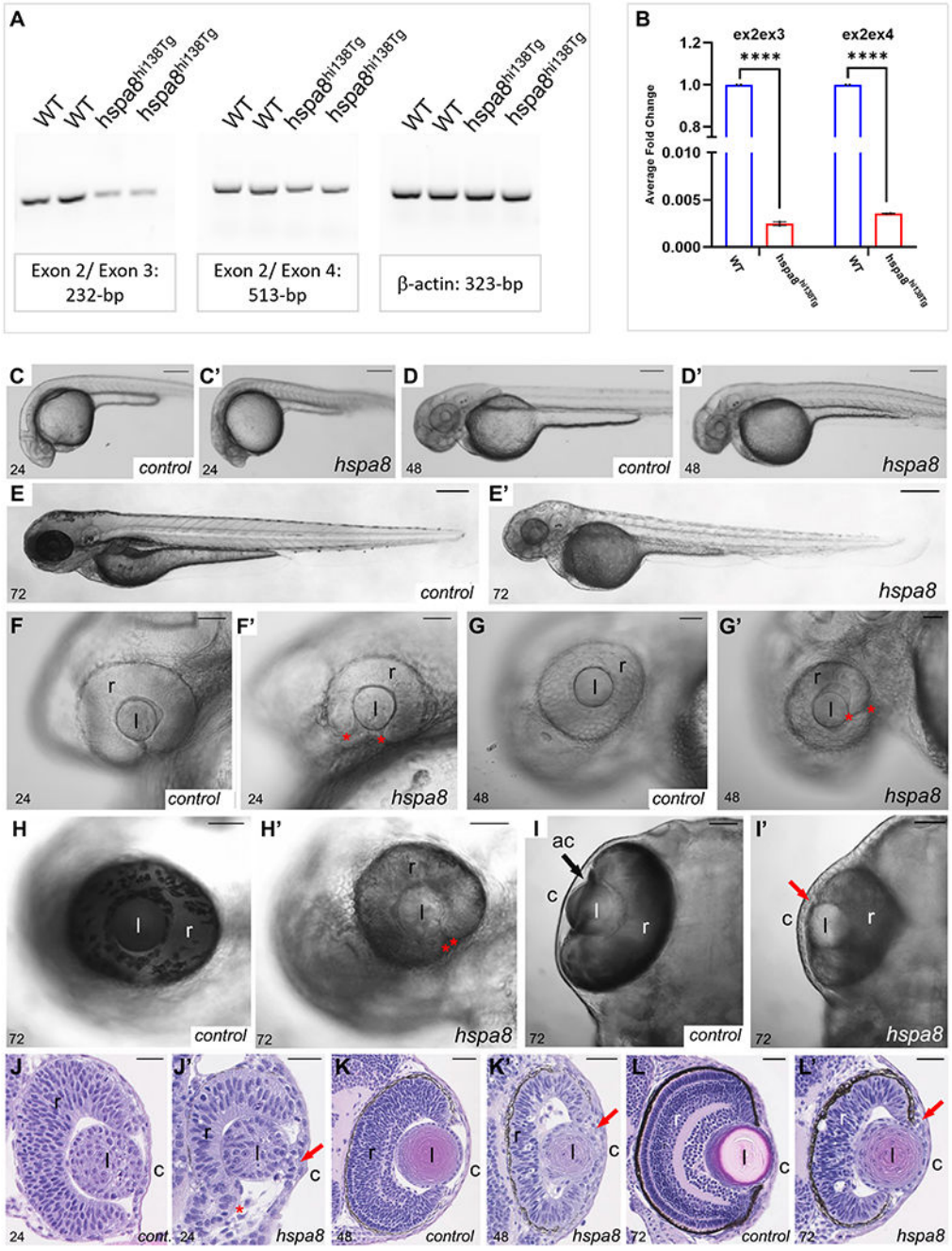


**Figure 3: Molecular and phenotypic characterizaton of homozygous *hspa8*$^{hi138Tg}$ zebrafish embryos.**

**A**. RT-PCR analysis of *hspa8* transcript level comparing 48-hpf wild-type and homozygous *hspa8*$^{hi138Tg}$ embryos. Two different primer sets were utilized; primer set one targeted exons 2 and 3, primer set two targeted exons 2 and 4. β-actin was used as a loading control.

**B**. qRT-PCR analysis of the *hspa8* transcript level utilizing two different primer sets (as utilized in RT-PCR experiments) comparing 48-hpf wild-type and homozygous *hspa8*$^{hi138Tg}$ embryos. Error bars indicate standard error of the mean (SEM). **** indicates statistical

significance with a P value <0.0001. **C-I'**. Gross morphological assessment of 24-, 48- and 72-hpf control and homozygous *hspa8*$^{hi138Tg}$ embryos (stage is marked in the left corner and type (control/*hspa8* mutant) in the right corner of each image). Homozygotes displayed systemic defects (small head, misshapen body); ocular defects included small, colobomatous eyes at all stages (red asterisks indicate retinal edges in F', G' and H'). At 72-hpf, homozygotes displayed severely reduced anterior chamber space and thickened corneas (compare black arrow in I to red arrow in I'). **J-L'.** H&E staining of transverse sections from 24- , 48- , and 72-hpf wild-type and homozygous *hspa8*$^{hi138Tg}$ embryos. At 24-hpf embryos display abnormally shaped optic cup (red asterisk in J') and lens-cornea attachment (red arrow in J'). At 48- and 72-hpf, small disordered retina, thick cornea and reduced anterior chamber space are observed (red arrow in K' and L'). (r) retina, (l) lens, (c) cornea, (ac) anterior chamber. Size of scale bar for C-I' is 200μm and for J-L' is 25μm.

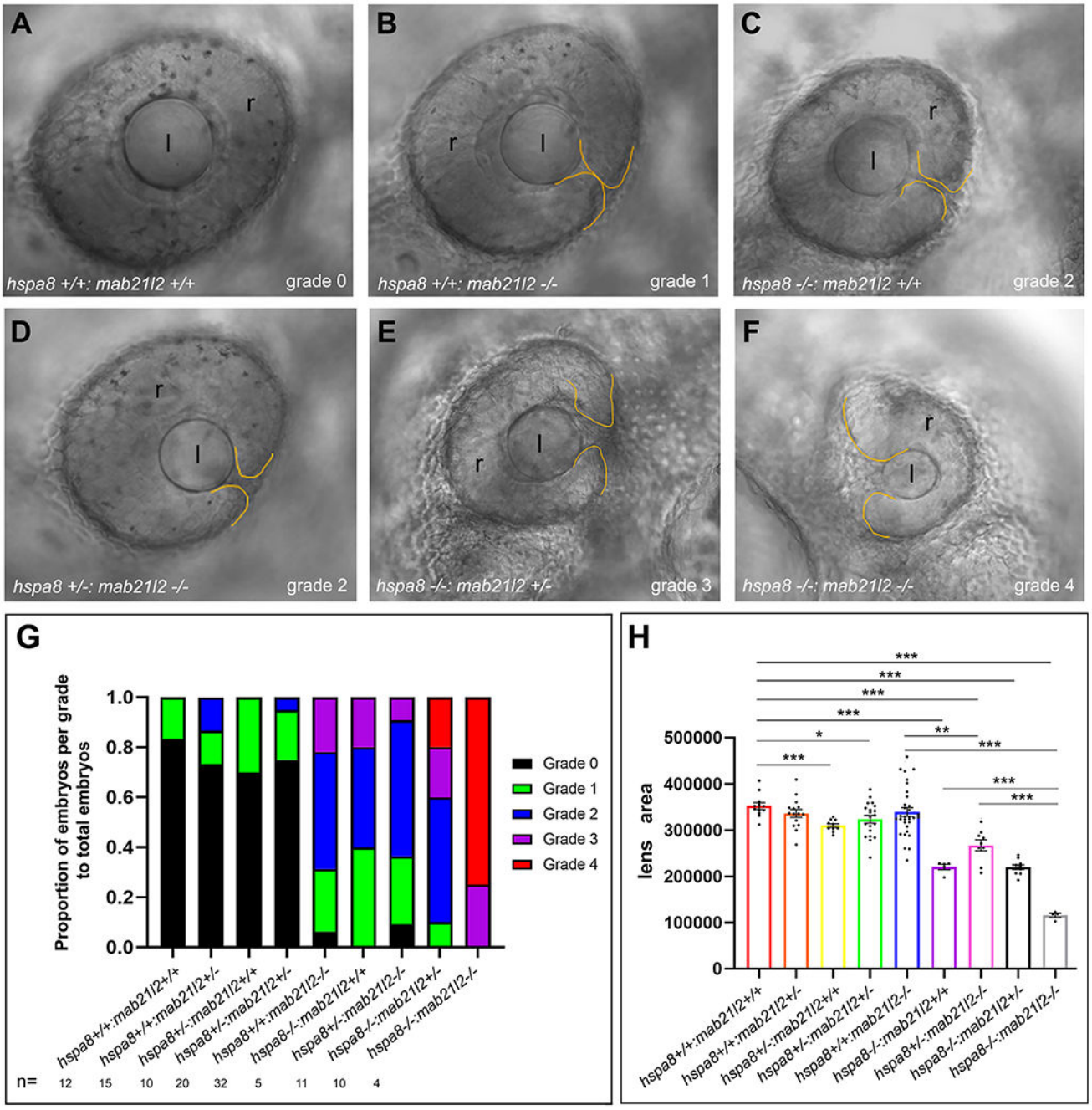


**Figure 4. Gross phenotypic analysis of *hspa8*$^{hi138Tg}$ and *mab21l2*$^{mw702}$ (*mab21l2*$^{Arg51\_Phe52del}$) double mutants.**

**A-F**. Representative images of 48-hpf embryos with various *hspa8*$^{hi138Tg}$ and *mab21l2*$^{mw702}$ allelic combinations; specific genotypes (left corner) and assigned grade for coloboma (right) are indicated; retinal margins are indicated with yellow outline. **G**. Graph of the proportion of embryos per grade to total embryos per allele combination. Grade 0 shown in black, grade 1 in green, grade 2 in blue, grade 3 in purple and grade 4 in red. **H**. Graph of average lens area per allele combination. Error bars indicate SEM. P values are indicated

above each bracket, with significance determined by a P value <0.05. (*** <0.0001; ** <0.0005; * <0.05).

**Table 1:**

Summary of MAB21L2 interacting proteins independently identified in Y2H assays.

| Gene Symbol | MAB21L2-WT v. Human Retina | | MAB21L2-WT v. Zebrafish Embryo | | mab21l2-wt v. Zebrafish Embryo | | MAB21L2-Arg51Gly v. Zebrafish Embryo | | Protein Name | Subcellular location[1,2] |
|---|---|---|---|---|---|---|---|---|---|---|
| | CS | SID | CS | SID | CS | SID | CS | SID | | |
| ARIH2/ arih2 | C | 170-393 | C | 223-427 | | | | | E3 ubiquitin-protein ligase | N |
| evi5b | | | D | 169-682 | D | 169-682 | D | 169-682 | Ecotropic viral integration site 5 homolog | N |
| hnf4a | | | C | 159-378 | B | 132-351 | C | 159-381 | Hepatocyte nuclear factor 4-alpha | N |
| **klhl31** | | | **A** | **52-262** | **A** | **50-262** | **A** | **52-264** | **Kelch-like protein 31** | **N** |
| mcm5 | | | D | 592-721 | D | 592-721 | C | 595-715 | DNA replication licensing factor | N, C |
| nop56 | | | D | 62-319 | B | 167-319 | | | Nucleolar protein 56 | N |
| nup205 | | | D | 230-606 | D | 230-606 | | | Nuclear pore complex protein | N |
| pdcd11 | | | D | 1449-1617 | D | 1448-1616 | | | Protein RRP5 homolog | N |
| pparab | | | D | 66-459 | D | 66-459 | | | Peroxisome proliferator-activated receptor alpha | N |
| psme4b | | | D | 1590-1827 | D | 1597-1827 | | | Proteasome activator complex subunit 4 | N, C |
| ranbp9 | | | C | 18-393 | D | 1-451 | C | 42-393 | Ran-binding protein 9 | N |
| STAT3/ stat3 | D | 1-705 | D | 53-539 | D | 53-539 | | | Signal transducer and activator of transcription 3 | N |
| **tnpo1** | | | **B** | **131-553** | **B** | **131-553** | **A** | **131-553** | **Transportin-1** | **N** |
| **TNPO2/ tnpo2** | **A** | **212-484** | **A** | **283-474** | **A** | **198-478** | **A** | **209-478** | **Transportin-2** | **N** |
| ANKFY1/ ankfy1 | D | 617-949 | | | D | 134-468 | | | Rabankyrin-5 | C |
| ckap5 | | | D | 1299-1682 | D | 1299-1682 | D | 1299-1682 | Cytoskeleton-assoc. protein 5 | C; c-skel. |
| DSP/dspa | D | 1814-1997 | D | 1150-1602 | | | | | Desmoplakin | C-skel, M |
| eif3ba | | | D | 53-339 | D | 125-387 | | | Eukaryotic translation initiation factor | C |
| etf1 | | | D | 130-341 | C | 130-340 | B | 138-340 | Eukaryotic peptide chain release factor | C |
| hook3 | | | D | 349-717 | D | 349-717 | | | Protein Hook homolog 3 | C; c-skel. |
| **KLC2/klc2** | **B** | **1-150** | **A** | **1-130** | **A** | **58-155** | **A** | **58-130** | **Kinesin light chain 2** | **C; c-skel.** |

| Gene Symbol | MAB21L2-WT v. Human Retina | | MAB21L2-WT v. Zebrafish Embryo | | mab21l2-wt v. Zebrafish Embryo | | MAB21L2-Arg51Gly v. Zebrafish Embryo | | Protein Name | Subcellular location[1,2] |
|---|---|---|---|---|---|---|---|---|---|---|
| | CS | SID | CS | SID | CS | SID | CS | SID | | |
| myo1eb | | | D | 715-1096 | D | 715-1096 | D | 715-1096 | Unconventional myosin-Ie | C; c-skel. |
| **SPTBN1/ sptbn1** | **D** | **507-681; 939-1326** | **B** | **590-667** | **D** | **254-710; 953-1345** | **D** | **474-667** | **Spectrin beta chain** | **C; c-skel., N** |
| trim71 | | | D | 267-500 | D | 265-563 | | | E3 ubiquitin-protein ligase | C |
| PNPLA6/ pnpla6 | D | 761-930 | | | D | 712-903 | | | Patatin-like phospholipase domain-containing protein 6 | C; ER |
| VPS35/ vps35 | D | 5-734 | | | D | 238-656 | | | Vacuolar protein sorting-assos. protein | C |
| ephb6 | | | D | 621-798 | D | 723-886 | | | Ephrin type-B receptor 6 | ECM |
| lygl2 | | | D | 4-191 | D | 4-191 | | | Lysozyme g | ECM |
| tnc | | | D | 1245-1542 | D | 1094-1359 | D | | Tenascin | ECM |
| sdhb | | | D | 40-237 | D | 40-237 | | | Succinate dehydrogenase iron-sulfur subunit | Mito |

[1] uniprot.org;

[2] Tang et al., 2003;

CS: confidence score; SID: selected interaction domain; ECM extracellular matrix; ER: Endoplasmic reticulum; C: cytoplasm; c-skel.: cytoskeleton; M: membrane; Mito: mitochondrion; N: nuclear. Interactions identified in three or more independent screens AND with CS between A-C in at least one screen are indicated in bold.

**Table 2:**

Summary of unique interactions identified for MAB21L2-Arg51Gly in Y2H assays.

| Gene Symbol | MAB21L2-WT v. Human Retina | MAB21L2-WT v. Zebrafish Embryo | mab21l2-wt v. Zebrafish Embryo | MAB21L2-Arg51G v. Zebrafish Embryo | | Protein Name | Subcellular location[1] |
|---|---|---|---|---|---|---|---|
| | | | | CS | SID | | |
| gli2a | - | - | - | D | 441-847 | Zinc finger protein | N |
| cux2a | - | - | - | D | 1-325 | Cut-like homeobox 2 | N |
| dnajc7 | - | - | - | D | 39-267 | DnaJ homolog subfamily C member 7 | N |
| **hspa5** | - | - | - | **C** | **279-508** | **Heat-shock 70 kDa protein 5** | **C, N** |
| **hspa8** | - | - | - | **A** | **255-420** | **Heat shock cognate 71 kDa protein** | **N** |
| ik | - | - | - | D | 77-319 | IK cytokine, downregulator of HLA II | N |
| kif4 | - | - | - | C | 871-970 | Chromosome-associated kinesin | N |
| kntc2l | - | - | - | D | 160-367 | Kinetochore protein NDC80 homolog | N |
| kpnb3 | - | - | - | D | 517-795 | Importin-5 | N |
| mphosph8 | - | - | - | D | 574-856 | M-phase phosphoprotein 8 | N |
| prdm15 | - | - | - | D | 743-1047 | PR domain zinc finger protein 15 | N |
| prpf40a | - | - | - | D | 382-602 | Pre-mRNA-processing factor 40 homolog A | N |
| prr12a | - | - | - | D | 2259-2493 | Proline-rich protein 12 | N |
| psme3 | - | - | - | D | 61-241 | Proteasome activator complex subunit 3 | N |
| rarab | - | - | - | D | 65-359 | Retinoic acid receptor alpha | N |
| sfpq | - | - | - | C | 226-494 | Splicing factor, proline- and glutamine-rich | N |
| trip12 | - | - | - | D | 314-585 | E3 ubiquitin-protein ligase TRIP12 | N |
| hsp90b1 | - | - | - | D | 418-750 | Endoplasmin | C; ER |
| cita | - | - | - | D | 1562-1947 | Non-specific serine/ threonine protein kinase | C; C-skel. |
| klc4 | - | - | - | D | 37-136 | Kinesin light chain 4 | C-skel. |
| stom | - | - | - | D | 990-1359 | Stomatin | C-skel., M |
| utrn | - | - | - | D | 1855-2231 | Utrophin | C-skel., M |
| blzf1 | - | - | - | C | 161-394 | Golgin-45 | Golgi |
| zgc:66014 | - | - | - | D | 237-507 | RAB11-binding protein RELCH homolog | Endosome, Golgi |
| irig1 | - | - | - | D | 346-604 | Leucine-rich repeats and immunoglobulin-like domains protein 1 | M |
| gfm1 | - | - | - | B | 557-724 | Elongation factor G, mitochondrial | Mito |

| Gene Symbol | MAB21L2-WT v. Human Retina | MAB21L2-WT v. Zebrafish Embryo | mab21l2-wt v. Zebrafish Embryo | MAB21L2-Arg51G v. Zebrafish Embryo | | Protein Name | Subcellular location[1] |
|---|---|---|---|---|---|---|---|
| | | | | CS | SID | | |
| fam83fa | - | - | - | D | 63-555 | Protein FAM83F | UNK |

[1] uniprot.org;

CS: confidence score; SID: selected interaction domain; ER: Endoplasmic reticulum; C: cytoplasm; C-skel: cytoskeleton; M: membrane; Mito: mitochondrion; N: nuclear; UNK: unknown